DOI: 10.17344/acsi.2023.8136 *Acta Chim. Slov.* **2023,** *70,* 479–488

Scientific paper

A novel nickel(II) Complex with N,S-donor Schiff Base: Structural Characterisation, DFT, TD-DFT Study and Catalytic Investigation

Manas Chowdhury,[1] Niladri Biswas,[1,2] Sandeepta Saha,[1,3] Ennio Zangrando,[4] Nayim Sepay[5] and Chirantan Roy Choudhury*,[1]

[1] *Department of Chemistry, West Bengal State University, Barasat, Kolkata-700126, India*

[2] *Department of Biotechnology, Institute of Genetic Engineering, No. 30, Thakurhat Road, Badu, Madhyamgram, Kolkata, West Bengal 700128, India*

[3] *Sripur High School, Madhyamgram Bazar, Kolkata-700130, India*

[4] *Department of Chemical and Pharmaceutical Sciences, University of Trieste, 34127 Trieste, Italy*

[5] *Department of Chemistry, Lady Brabourne College, Kolkata-700017, India.*

** Corresponding author: E-mail: crchoudhury2000@yahoo.com;*
Tel: + 91-9836306502; Fax: +91-33-2524-1577

Received: 03-012-2023

Abstract

One new mononuclear nickel(II) thiosemicarbazone complex (**1**), has been synthesised from the Schiff base ligand derived from *p*-anisaldehyde and thiosemicarbazide. Complex **1** was characterized by using different spectroscopic techniques and single crystal X-ray structural analysis. The time dependent density functional theory (TD-DFT) was applied to simulate the electronic spectra of the complex **1** with the help of Polarizable Continuum Model (PCM). Complex **1** acts as functional model towards catechole-oxidase activity and the catalytic property has been evaluated from Lineweaver-Burk plot using the Michaelis-Menten approach of enzyme catalysis with a k_{cat} value of the order of 708 h^{-1}.

Keywords Catecholase-like activity, crystal structure, DFT study, Ni(II) complex, Schiff base

1. Introduction

Biomimetic models of metalloenzymes have emerged as an important class of compounds for their application to catalytic organic conversions which are otherwise difficult to achieve.[1–4] In catechole-oxidase metalloenzyme one hydroxide ion forms a bridge between the dinuclear copper(II) active site.[5–6] Among different Schiff bases, thiosemicarbazones are considered as extremely suitable ligands for their different coordination behaviour, as it can bind in both anionic as well as neutral form.[7–10] Various copper(II) complexes showing catechol- oxidase activity have been reported[11–13] along with complexes of other transition metals such as manganese(II),[14] nickel(II),[15] iron(III),[16] cobalt(II/III),[5,17] and zinc(II).[18] In particular it was observed that catecholase-like activity was exhibited by metal complexes comprising of ligands with *N,N-*, *N,O-* or *N,S*-donor set.[19–25]

Till date dinuclear nickel(II) metal complexes have been frequently studied for their catecholase activity,[26–29] but systematic reports of mononuclear nickel(II) complexes which can be used as catecholase mimicking systems are less reported.[30,31] These facts prompted us to synthesise a nickel(II) complex with the Schiff base ligand 2-(4-methoxybenzylidene)hydrazine-1-carbothioamide(HL) bearing both hard and soft *N,S*-donor site (Scheme 1). The present Ni(II) complex has been reported earlier together with Cu and Pd derivative containing the same ligand, but not supported by X-ray single crystal analysis.[32]

The catalytic efficiency of the complex **1** towards catecholase-like activity was studied in detail and it was revealed that it is an efficient species for the oxidation of

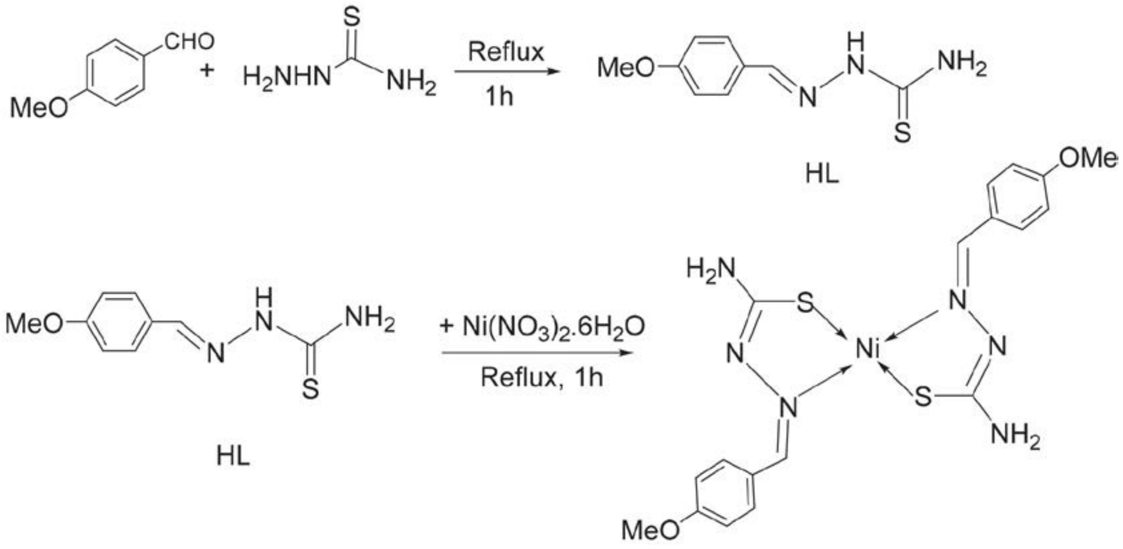

Scheme 1. Synthesis of ligand HL and complex **1.**

3,5-di-*tert*-butylcatechol (3,5-DTBC) to 3,5-di-*tert*-butylbenzoquinone (3,5-DTBQ) (Scheme 2).

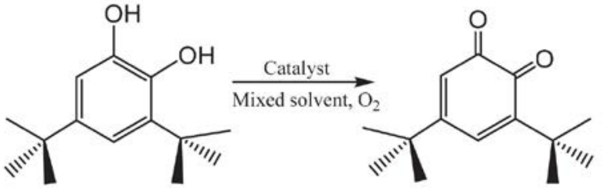

Scheme 2. Catecholase-like activity exhibited by the complex **1**.

2. Experimental Section

2. 1. Materials

All materials were of reagent grade and were used without further purification. Nickel(II) nitrate hexahydrate [$Ni(NO_3)_2·6H_2O$], thiosemicarbazide (Sigma Aldrich), and *p*-anisaldehyde (Sigma-Aldrich) were used as received.

2. 2. Physical Techniques

Fourier Transform Infrared spectrum (4000–400 cm^{-1}) of the complex **1** was recorded on a Perkin-Elmer SPECTRUM-2 FT-IR spectrophotometer in solid KBr matrices. Electronic spectrum was recorded at 300 K on a Perkin-Elmer Lamda-35 UV-Vis spectrophotometer in DMSO. C, H, N microanalyses were carried out with a Perkin-Elmer 2400 II elemental analyzer. Electrochemical studies were performed in DMSO with a CH 660E cyclic voltammeter at a scan rate of 50 mV sec^{-1} by using saturated calomel electrode (SCE) as a reference in a three-electrode system and tetrabutylammonium perchlorate as supporting electrolyte. Nitrogen gas was bubbled through the sample solution at a constant rate for 1 minute.

2. 3. Synthesis

2. 3. 1. Synthesis of Schiff Base (HL)

A methanolic solution of *p*-anisaldehyde (608.35 μL, 5 mmol) was added to a methanolic solution of thiosemicarbazide (0.4557 g, 5 mmol) in same ratio and the reaction mixture was refluxed for two hours. Then the reaction mixture was cooled at room temperature and used without further purification.

2. 3. 2. Synthesis of Nickel(II) Complex (1)

$Ni(NO_3)_2·6H_2O$ (0.183 g, 1 mmol) in methanol medium was added into the solution of the Schiff base in 1:1 millimolar ratio and the reaction mixture was refluxed for two hours. Then the solution was filtered and left for slow evaporation. After a few days, brown coloured single crystals were obtained and separated out. Yield: 68%. Anal. Calc. for [$C_{18}H_{20}N_6NiO_2S_2$]: C, 45.45; H, 4.21; N, 17.68% Found: C, 45.41; H, 4.18; N, 17.66%. IR bands: (ν, cm^{-1}) 1609 ν(C=N); 560 ν(Ni-N); 493 ν(Ni-S), 671 ν(C-S), 3466 ν(O-H). UV-Vis: λ_{max} (nm) (DMSO): 283, 401, 565.

2. 3. 4. Crystallographic Data Collection and Refinement

Diffraction data collection of the complex **1** was performed at the X-ray diffraction beam line (XRD1) of the Elettra Synchrotron of Trieste (Italy), with a Pilatus2M image plate detector. Complete dataset was collected at 100(2) K with a monochromatic wavelength of 0.7000 Å. The diffraction data were indexed, integrated, and scaled using XDS.[33] The structure was solved by direct methods using SIR2014.[34] Fourier analysis and refinement were performed by the full-matrix least-squares methods based on F^2 implemented in SHELXL-2019/2.[35] All non-hydrogen atoms were refined anisotropically. The molecular graphics and crystallographic illustrations complex were prepared using DIAMOND 4[36] program. All the relevant crystallographic data and details of structure refinement are summarized in Table 1.

Table 1. Crystal data and details of structure refinement of complex **1**.

empirical formula	$C_{18}H_{20}N_6NiO_2S_2$
formula weight (g mol^{-1})	475.23
Crystal system	Monoclinic
Space group	$P2_1/c$
a (Å)	12.473(3)
b (Å)	5.5140(11)
c (Å)	14.195(3)
β (deg)	101.88(3)
V (Å^3)	955.4(3)
Z	2
d_{calc} (g cm^{-3})	1.652
M (mm^{-1})	1.203
F(000)	492
crystal size (mm^3)	0.11 × 0.30 × 0.32
Collected reflections	29501
Independent reflections	2907
R_{int}	0.0264
Goodness-of-fit on F^2	1.099
Final R_1, wR_2 indices [$I > 2\sigma(I)$]	0.0272, 0.0684
R_1, wR_2 indices (all data)	0.0279, 0.0689
Residuals (eÅ^{-3})	0.505, −0.597

2. 3. 5. DFT Studies

The energy minimized structure of the complex **1** (in the isolated form) was obtained using density functional theory (DFT) calculation. For this study, B3LYP dispersion corrected hybrid functional along with mixed basis sets LANL2DZ for Ni(II) ion and 6-311G(d,p) for other atoms were used with spin-unrestricted scheme. The initial coordinates for structure optimization were taken from the X-ray crystallographic structure. The Gaussian 09 software with D1 revision and Gauss View5[37,38] were used for DFT calculations and molecular visualization software, respectively. Using the optimized structure, the electronic absorption spectrum, at the same level of theory, was calculated in DMSO solvent using the Polarizable Continuum Model (PCM). Frontier molecular orbitals (FMOs) like HOMO and LUMO were drawn by Gauss View6. Gauss Sum was utilized to get the contribution of orbitals and outcome obtained in TD-DFT.

3. Result and Discussion

3. 1. Infrared Spectra Study

The FT-IR-spectrum of complex **1**, shown in Fig. S1, exhibited a distinctive band at 1609 cm^{-1}, which can be assigned to the C=N [39] stretching frequency of azomethine group. The bands at 560 and 493 cm^{-1} are due to the formation of Ni-N and Ni-S bonds[39,40] and the band detected in the region of 671 cm^{-1} can be attributed to the C-S stretching frequency.[41] In addition, the complex showed a prominent IR band at 3466 cm^{-1}due O-H stretching frequency.

3. 2. Electronic Spectral Study

The electronic spectrum of complex **1** in DMSO solution at a concentration of 10^{-3} M is shown in Fig. S2. The complex exhibited three characteristics peaks in the region 283–565 nm. The sharp high intensity band observed at 283 nm can be attributed to **π→π*** transition[42] of coordinated imine of the ligand. A moderate intense peak observed at 401 nm was assigned to **n→π*** transition[43] and a very low intensity band, detected at 565 nm correspondent to d→d transition. The electronic spectrum of **1** was carried out for three successive days maintaining same concentration and same solvent, but no significant change was detected.

3. 3. Cyclic Voltammetric Study

The cyclic voltammogram of complex **1** (displayed in Fig. S3) shows one irreversible oxidative peak at +1.30 V (versus SCE) in the anodic region that can be attributed to the oxidation of Ni(II) to Ni(III). The irreversible reductive peak at −0.65 V (versus SCE) in the cathodic region is due to the reduction of Ni(II) to Ni(I).

3. 4. Structural Description

Brown single crystals of complex **1** were obtained by slow evaporation of a saturated methanolic solution. The X-ray structural analysis shows that the geometry of complex **1** is square planar.

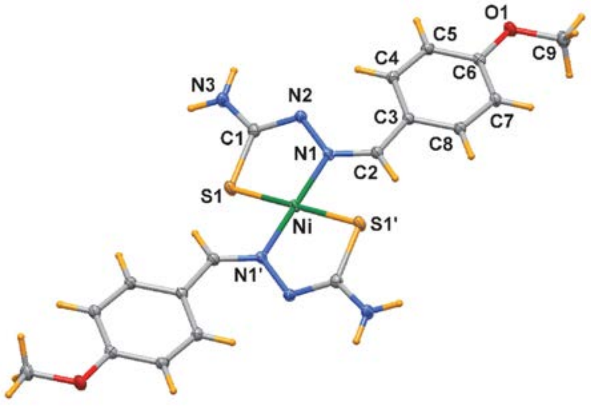

Fig. 1. ORTEP diagram (ellipsoid probability at 50%) of the centrosymmetric complex **1** (primed atoms at −x, −y + 1, −z + 1).

The molecular structure consists of a centrosymmetric neutral complex species [Ni(L)$_2$], with the nickel atom located at an inversion center, so that the asymmetric unit comprises only half complex. An ORTEP view of the complex along with the atom numbering scheme is depicted in Fig. 1 and a selection of bond lengths and angles is given in Table 2 and 3, respectively, along with calculated values obtained from the DFT approach. The thiosemicarbazone ligands chelate the Ni(II) center via *N,S*-donor atoms in trans configuration resulting in two five membered rings. The Ni–N1 and Ni–S1 bond distances are of 1.9210(12) and 2.1820(5) Å with a chelating angle of 84.83(4)°. The ligand atoms are not coplanar and the phenyl ring forms a dihedral angle of 23.22(6)° with the coordination plane NiN_2S_2. These bonding parameters are in good agreement with the coordinating pattern of similar square planar Ni complexes with thiosemicarbazone ligands,[44] where Ni–N and Ni–S bond distances were found in to fall in the range 1.906(2) –1.9310(19) and 2.1735(7) –2.1796(6) Å, respectively.

Table 2. Experimental and DFT calculated bond distances (Å) for complex **1.**

	Complex **1**	
Bond distances	**X-ray**	**DFT**
Ni–N1	1.9210(12)	1.9522
Ni–S1	2.1820(5)	2.1142

Table 3. Experimental and DFT calculated bond angles (°) for complex **1.**

	Complex **1**	
Bond angles	**X-ray**	**DFT**
S1–Ni–N1	84.83(4)	84.42
S1–Ni–S1^i	180.00	180.00
S1–Ni–N1^i	95.17(4)	95.64
N1–Ni–N1^i	180.00	180.00

Symmetry code for primed atoms: $-x, -y + 1, -z + 1$

Upon coordination the bond lengths in thiosemicarbazone ligand undergo some changes compared to the values measured in the free ligand.[44] In particular, the C1–S1 bond length of 1.670(2) Å elongates to 1.7387(14) Å, while the C1–N2 bond distance from 1.350(2) Å shortens to 1.3000(17) Å in the complex. These features are consistent with the acquisition of a partial single bond character in the former, and a partial double bond in the latter.

In addition, the square-planar coordination geometry with the N_2S_2 donor atoms involves the thiolato sulphur and the nitrogen N1 atoms in *Z* configuration (Fig. 1) indicating that the complexation occurs after a 180° rotation around the C1–N2 bond.[44]

The crystal packing evidences phenyl rings π-stacking with distance between centroids of 3.6343(11) Å, in addition to weak H bonds involving the amino group NH_2 with O1 leading to a 2D supramolecular network (N3···O1 = 3.0962(18) Å) as shown in Fig 2. Finally, the amino group NH_2 interact also with S1 (N3···S1= 3.5493(18) Å) giving rise a 3D architecture.

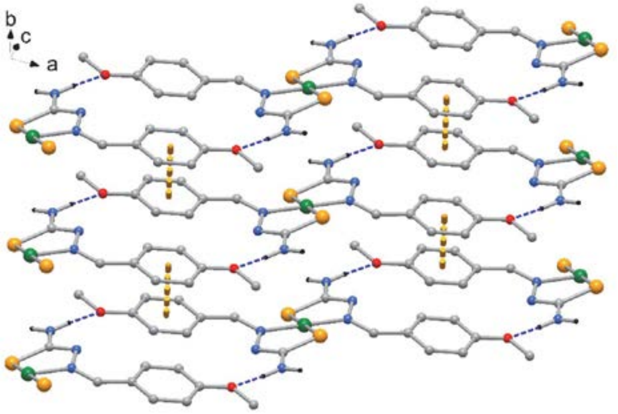

Fig. 2. Detail of crystal packing of complex **1** with indication of π-stacking between phenyl ring and N-H···O hydrogen bonds (only H atoms at N3 are shown for clarity).

3. 5. DFT Studies

Density functional theory approach can be used to evaluate the experimental properties of the complex.[45] The structure of the complex **1** obtained from X-ray crystallography was optimized with the help of DFT method leading to a self-consistent field total energy and dipole moment of –3588436.369697 kJ/mol and 0.005993 Debye, respectively. The structure of the complex **1** obtained after energy minimization is reported in Fig. 3a. Atom-by-atom overlay of asymmetric unit of X-ray crystal structure (orange) with energy minimized structure (violet) of the complex is displayed in Fig 3b. The difference of root mean square deviation of these structures was found to be 0.3623 Å, and most of the bond lengths and angles of the optimised structures corroborates with those of the corresponding X-ray structure. Few changes were observed for the atoms in the coordination sphere of the Ni center. The bond distances Ni–S, C–S, C=N, N–N, and N–Ni in the crystal structure are 2.18, 1.74, 1.31, 1.39, and 1.92 Å, respectively, whereas they are 2.11, 1.54, 1.42, 1.44, and 1.95, respectively, in the case of optimised structure. Such structural differences can be attributed to the fact the experimental structure is obtained in the solid state and theoretical structure obtained in vacuum.

The electronic spectrum of the complex **1** was simulated in the DMSO medium by using the time dependent density functional theory (TD-DFT) and compared with the experimental one. The simulated spectrum shows a strong absorption band at λ_{max} = 410 nm (oscillator strength 0.87), while the complex shows an absorption band at λ_{max} = 401 nm (Fig. 3c). The TD-DFT calculation shows that HOMO to LUMO (99%) and HOMO-1 to LU-

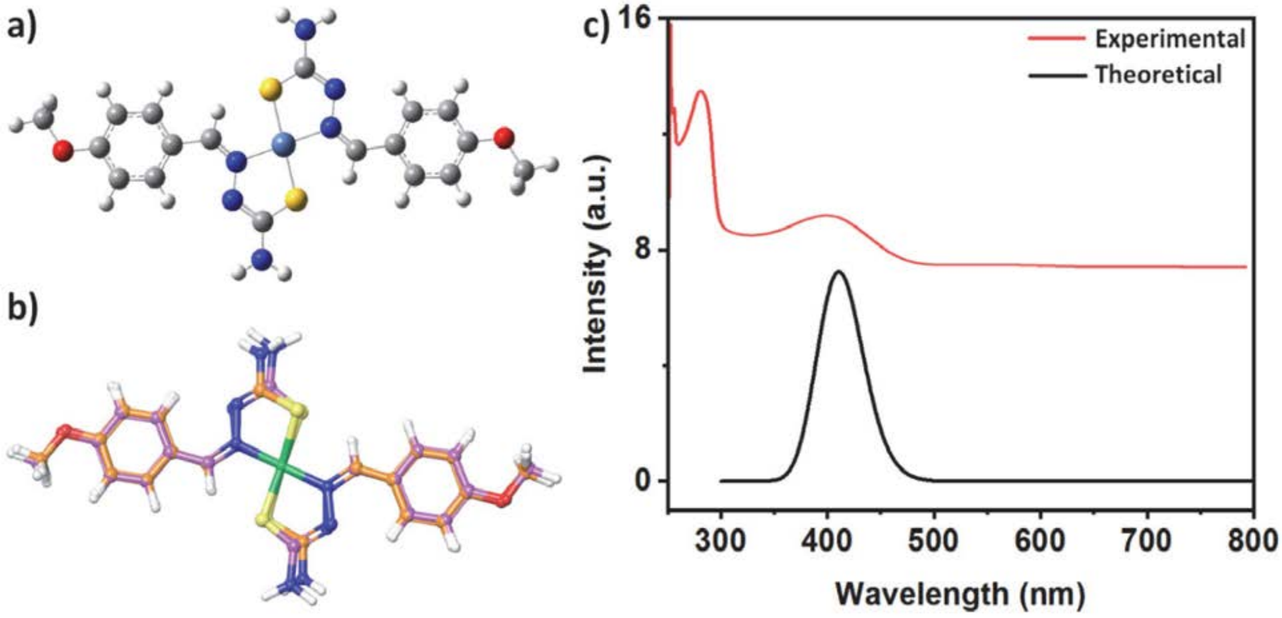

Fig. 3. (a) DFT energy minimized structure of the complex **1**, (b) overlay of energy minimized (violet) and X-ray crystal structure (orange) of the complex **1**, and (c) experimental and theoretical absorption spectra of the complex **1**.

MO transition are responsible for the above mentioned absorption band.

In the formation of metal complexes, energy and electron density in the complexes show drastic changes from those of the ligand. The chemical reactivity of a molecule depends upon the difference in energy between the highest occupied molecular orbital (HOMO) and lowest unoccupied molecular orbital (LUMO).[46] In fact, high energy of HOMO facilitates the interaction of the molecule with other molecules through electron donation whereas, molecule with low energy LUMO can accept electron easily from other molecules.[46,47] It is interesting to note that assembly of the Ni(II) ion with (*Z*)-2-(4-methoxybenzylidene)hydrazine-1-carbothioamide ligands induces lowering of the LUMO and enhancement of the HOMO energy with respect to the **HL** in the complex (Fig. 4). As a result, the energy gap between HOMO and LUMO of **HL** (2.09 eV) is much higher than that of the complex (1.14 eV). Therefore, the complex **1** is more soft in nature and capable of interaction with other molecules through both electron donation and electron acceptance. In addition, the electron density of HOMO is concentrated over the large planar aromatic moiety, while in the case of LUMO, it is spread also over Ni atom (d_{xy}). As a result, the complex **1** can accept electron very easily at the metal centre in LUMO. All the aforesaid electronic and energy features make the complex a good catalyst.

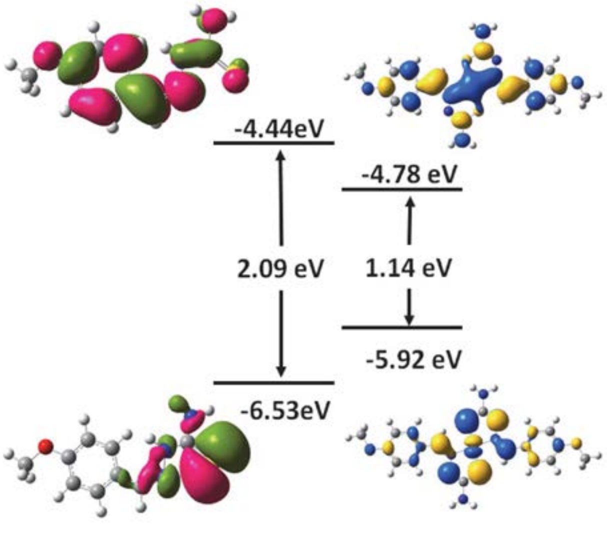

Fig. 4. HOMO and LUMO molecular orbitals and their energy of ligand and in complex **1.**

3. 6. Catecholase Activity

In order to assess the strength of the complex **1** to mimic the catecholase activity, the substrate 3,5-di-*tert*-butylcatechol (3,5-DTBC)[29] appears to be the most efficient substrate.[48] This molecule has allow redox potential that facilitates oxidation process and bears bulky *tert*-butyl substituents hindering any further over oxidation reaction and ring opening. The stability of the oxidised product 3,5-di-*tert*-butylbenzoquinone (3,5-DTBQ) is very high and the maximum absorption is shown at 400 nm in pure DMSO.[49]

3. 6. 1. Reaction with 3,5-DTBC as Substrate

A solution of 1×10^{-4} M of complex **1** in DMSO was mixed with a DMSO solution of 3,5-DTBC (1×10^{-2} M) at room temperature. The UV-Vis spectra of the mixture were recorded at regular intervals of 5 mins.[48] After addition of the complex **1** to the solution of 3,5-DTBC, a steady rise in absorbance was observed with the appearance of a new band at 402 nm, correspond to the formation of 3,5-di-*tert*-butylbenzoquinone (3,5-DTBQ) (Fig. 5).[50]

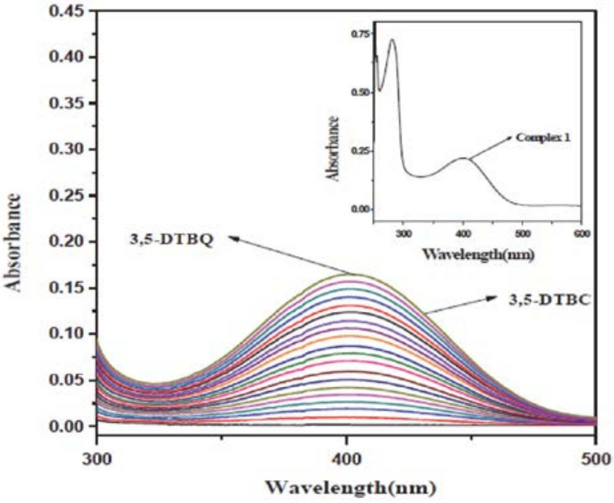

Fig. 5. Increase of the absorbance after the addition of 100 equivalents of 3,5-DTBC to a 10^{-4} M solution of complex **1**. The spectra were recorded at intervals of 5 min.

The $\log[A_\alpha/(A_\alpha - A_t)]$ versus time plot was utilised to determine the rate constant for a specific complex substrate mixture (Fig. 6).[48,49]

Since saturation kinetics is followed by initial rate methods at higher substrate concentration, the Michaelis–Menten model was used for the study of enzyme kinetics and the Lineweaver-Burk plot was employed to compute the various kinetics parameters for the complex **1**. The Michaelis binding constant (K_m), maximum velocity (V_{max}) values and the rate constant for the dissociation of the substrate (i.e. turnover frequency, K_{cat}) were all calculated from the Lineweaver–Burk graph $1/V$ vs. $1/[S]$ (Fig. 7) by utilizing the equation $1/V = \{K_m/V_{max}\}\{1/[S]\} + 1/V_{max}$.

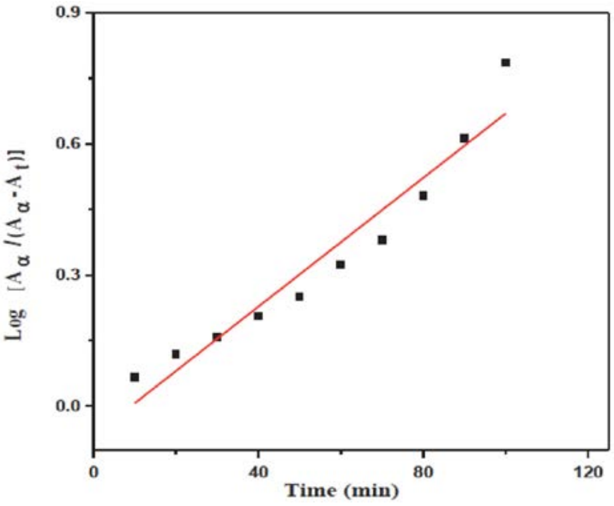

Fig. 6. Change in absorption maxima at 402 nm with time for complex **1**.

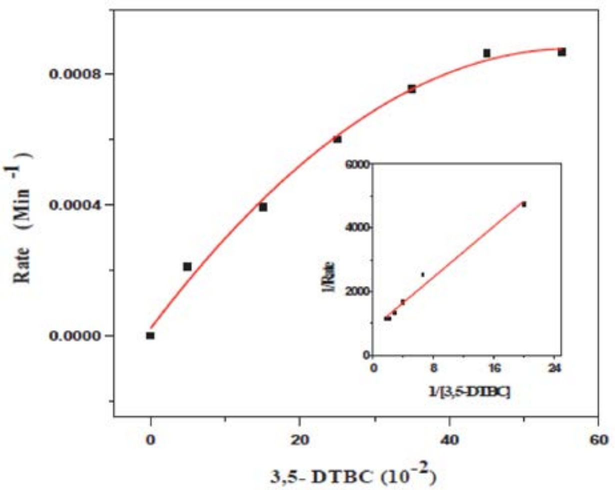

Fig. 7. Plot of rate vs substrate concentration for complex **1**. Inset shows the Lineweaver-Burk plot.

The V_{max}, K_m, and K_{cat} kinetic parameters for the complex **1** were found to be 1.18×10^{-3} M min^{-1}, 0.235 M and 708 h^{-1} respectively.[40,44,48,49,51]

Table 4. K_{cat} values for the oxidation of 3,5-DTBQ catalyzed by reported mononuclear Ni(II) complex along with other metal complexes.

Complex	Solvent	K_{cat}	References
$[Ni(L)_2]$ Complex **1**	DMSO	708	This work
$[Ru(PPh_3)Cl_2(L_2)]$	DMSO	2.346×10^3	23
$[Ni(L_3)]ClO_4$	CH_3OH	8×10^3	40
$[Ni(L_4)]ClO_4$	CH_3OH	2.7×10^3	40
$[Ni(L_5)_2]$	DMSO	116	44
$[Cu(L_6)(CCl_3COO)(H_2O)].H_2O$	DMSO	1452.00	48
$[Cu(L_7)(H_2O)Cl]_2$	DMSO	1458.00	48
$\{[Cu(HL_8)(H_2O)](NO_3)\}_n$	DMSO	5.19×10^3	49
$[Cu_2(L_8)_2(H_2O)_3]_n$	DMSO	5.56×10^3	49
$[Ni(L_9)_2]$	CH_3OH	140.72	50

Key: HL_2= (*E*)-4-chloro-2-(((2-(dimethylamino) ethyl)imino)methyl)phenol. HL_3= 1-Phenyl-3-(2-piperazin-1-yl-ethylimino)-but-1-en-1-ol. HL_4= 4-((2-(piperazin-1-yl)ethyl)imino)pent-2-en-2-ol. HL_5 = [N-(diethylaminothiocarbonyl)-benzimidoylchloride-2-aminoacetophenone-*N*-methylthiosemicarbazone]. HL_6 = Hpymab = (*E*)-2-((pyridine-2-yl)methyleneamino) benzoic acid. HL_7 = HPmyaib = (HPmyaib = 4-iodo-2-{(*E*)-[(pyridin-2-yl)methyleneamino}benzoic acid). [H_2L_8 = H_2Pymat = (*E*)-2-(1-(pyridin-2-yl)-methyleneamino) terephthalic acid]. HL_9 = 1,1'-(1*E*,1*E*)-(propane-1,3-diylbis(azan-1-yl-1-ylidene)bis(methan-1-yl-1-ylidine)dinaphthalene-2-ol.

3. 6. 2. Reaction Mechanism

The probable mechanism of 3,5-DTBC oxidation by complex **1** is shown in Scheme 3. When a mixture of starch and potassium iodide was added to a solution of the complex **1** and 3,5-DTBC, the formation of a blue colour indicate that H_2O_2 was produced during the progress of the reaction. Meanwhile it is noteworthy that no blue colouration was observed in presence of only 3,5-DTBC. The mechanism of formation of H_2O_2, obtained as a byproduct during the oxidation of 3,5-DTBC to 3,5-DTBQ catalysed by the complex **1** followed similar mechanism found in the literature.[52]

Following the generalized mechanism of catecholase reaction induced by the complex **1** (Scheme 3), it can be stated that the Ni(II) metal centre is the main facilitator for the transfer of electrons that delocalise more easily through the C=N bond of the Schiff base to the neighbouring conjugate system. In other words, the chelation of Schiff bases to the metal expands the aromatic system consisted of delocalized π-electrons with an achievable thione-thiol tautomerism (Scheme 3).[10]

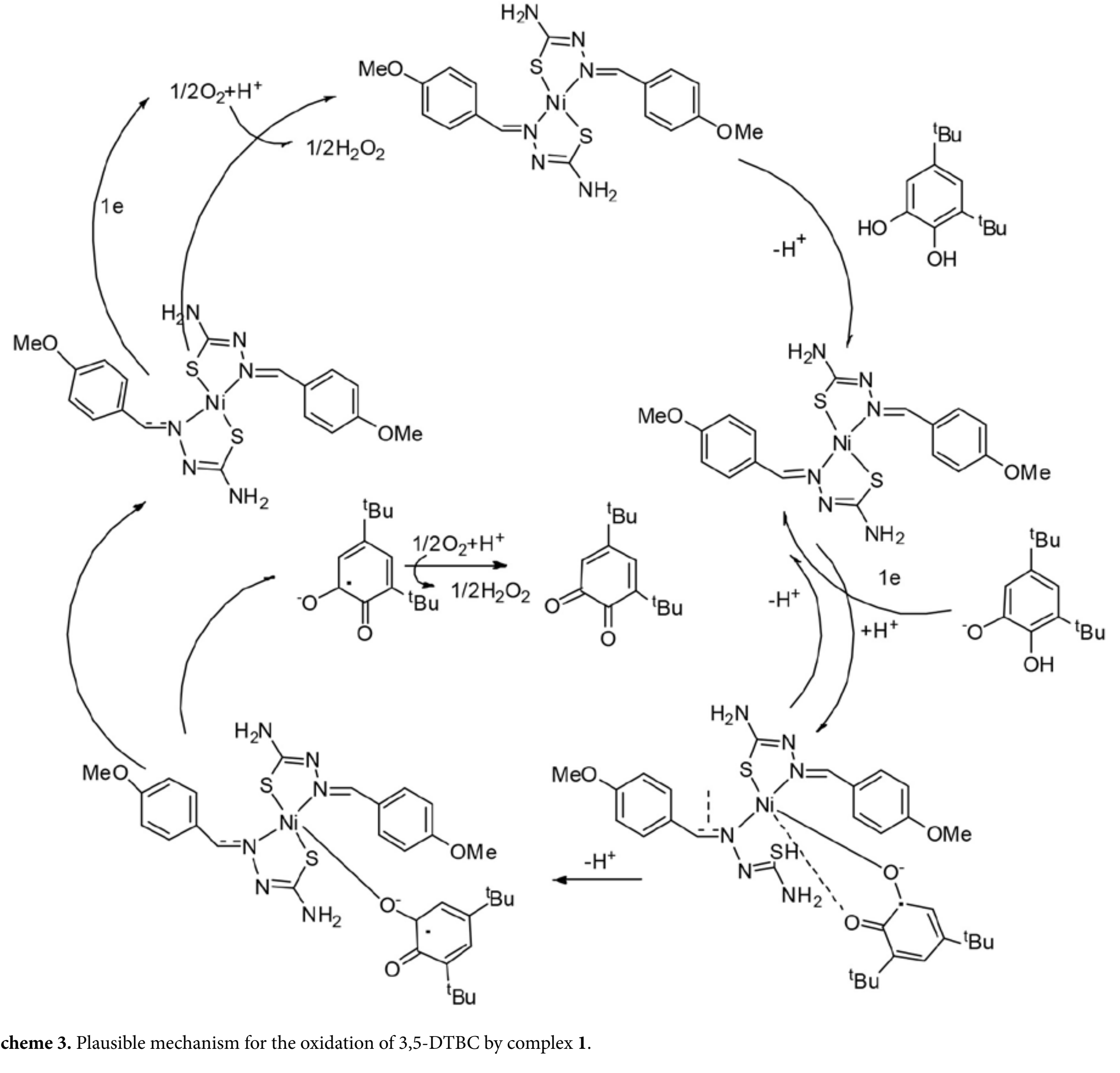

Scheme 3. Plausible mechanism for the oxidation of 3,5-DTBC by complex **1**.

3. 6. 3. Comparison with Previous Related Studies: Significant Aspects

Single crystal X-ray structure characterizations is of paramount importance to ascertain structure-property relationships.[19] In recent times, researchers have been describing many transition metal(II) systems to mimic Catecholase activity. Some of the metal complexes are mononuclear, while a large number of metal complexes are dinuclear in nature, and it was found that some model catalysts demonstrate high turnover number (K_{cat}), whereas opposite results were also presented.[20] Therefore, we can make a conclusive remark, as per the available data of the Table 4, that a simple relationship between the nuclearity of the system and the observed K_{cat} value is not possible due to numerous variables involved, such as metal-metal distance, flexibility and electronic/steric properties of the ligand, exogenous bridging ligand, and coordination geometry around the metal centre.[48,49]

4. Conclusion

(i) The present work focuses the synthesis and characterization of one nickel (II) thiosemicarbazone complex (1) of the Schiff base ligand (*Z*)-2-(4-methoxybenzylidene)hydrazine-1-carbothioamide (L) derived from *p*-anisaldehyde and thiosemicarbazide.
(ii) Complex **1** was well characterized by elemental analysis, cyclic voltammetry and spectroscopic measurements like FT-IR, UV-Vis spectroscopy, cyclic voltammetry along with single crystal X-ray analysis.
(iii) Time dependent density functional theory (TD-DFT) was performed to simulate the electronic spectra of the complex **1** with the help of Polarizable Continuum Model (PCM) which was further supported by Frontier molecular orbitals (FMOs).
(iv) Complex **1** exhibits significant catecholase activity towards the aerial oxidation of 3,5-di-tert-butyl catechol to the corresponding quinone in DMSO.

5. Acknowledgements

N. Biswas acknowledges CSIR, New Delhi, Govt. of India, for awarding junior research fellowship (Project No: 01/2537/11- EMR - II). M. Chowdhury acknowledges UGC, New Delhi, Govt. of India, for awarding Senior research fellowship (Sr. No. 2121410140, Ref. No. 21/12/2014 (II) EU-V). C. Roy Choudhury acknowledges DST- FIST (Project No. SR/FST/CSI-246/2012) New Delhi, Govt. of India for instrumental support under capital heads.

Appendix A. Supplementary data

CCDC 2239973 contains the supplementary crystallographic data for complex **1**. These data can be obtained free of charge via http://www.ccdc.cam.ac.uk/conts/retrieving.html, or from the Cambridge Crystallographic Data Centre, 12 Union Road, Cambridge CB2 1EZ, UK; fax: (+44) 1223-336-033; or e-mail: deposit@ccdc.cam.ac.uk. Supplementary data associated with this article can be found, in the online version, at http://

Disclosure statement

No potential conflict of interest was reported by the authors.

6. References

1. A. K. Maji, A. Chatterjee, S. Khan, B. K. Ghosh, *J. Mol. Struct.* **2017**, *1146*, 821–827. **DOI:**10.1016/j.molstruc.2017.06.077
2. S. K. Dey, A. Mukherjee, *Coord. Chem. Rev.* **2016**, *310*, 80–115. **DOI:**10.1016/j.ccr.2015.11.002
3. R. Rahaman, B. Chakraborty, T. K. Paine, *Angew. Chem. Int. Ed.* **2016**, *55*, 13838–13842. **DOI:**10.1002/ange.201607044
4. (a) S. K. Chatterjee, R. C. Maji, S. K. Barman, M. M. Olmstead, A. K. Patra, *Angew. Chem. Int.* Ed. **2014,** *53,* 10184–10189. **DOI:**10.1002/ange.201404133
   (b) S. Dasgupta, I. Majumder, P. Chakraborty, E. Zangrando, A. Bauzá, A. Frontera, D. Das, Eur. *J. Inorg. Chem.* **2017,** 133–145. **DOI:**10.1002/ejic.201600985
5. C. Eicken, B. Krebs, J. C. Sacchettini, *Curr. Opin. Struct. Biol.* **1999**, *9*, 677–683. **DOI:**10.1016/S0959-440X(99)00029-9
6. T. Klabunde, C. Eicken, J. C. Sacchettini, B. Krebs, *Nat. Struct. Biol.* **1998**, *5*, 1084–1090. **DOI:**10.1038/4193
7. B. Shaabani, A. A. Khandar, F. Mahmoudi, S. S. Balula, L. Cunha-Silva, *J. Mol. Struct.* **2013**, *1045*, 55–61. **DOI:**10.1016/j.molstruc.2013.03.049
8. N. Biswas, S. Khanra, A. Sarkar, S. Bhattacharjee, D. P. Mandal, A. Chaudhuri, S. Chakraborty, C. R. Choudhury, *New J. Chem***.** **2017**, *41*, 12996–13011. **DOI:**10.1039/C7NJ01998J
9. J. Haribabu, K. Jeyalakshmi, Y. Arun, N. S. P. Bhuvanesh, P. T. Perumal, R. Karvembu. *RSC Adv*. **2015**, *5*, 46031–46049. **DOI:**10.1039/C5RA04498G
10. N. Biswas, S. Saha, S. Khanra, A. Sarkar, D. P. Mandal, S. Bhattacharjee, A. Chaudhuri, S. Chakraborty, C. R. Choudhury, *J. Biomol. Struct. Dyn*. **2018**, *37*, 2801–2822. **DOI:**10.1080/07391102.2018.1503564
11. (a) M. Merkel, N. Moller, M. Piacenza, S. Grimme, A. Rompel, B. Krebs, *Chem. Eur.* J. **2005**, *11,* 1201–1209. **DOI:**10.1002/chem.200400768
    (b) B.Sreenivasulu, F. Zhao, S. Gao, J. J. Vittal, Eur. *J. Inorg. Chem.* **2006,** 2656–2670. **DOI:**10.1002/ejic.200600022
12. (a) S. Majumder, S. Sarkar, S. Sasmal, E. Carolina Sãnudo, S. S. Mohanta, Inorg. Chem. 2011, 50, 7540–7554. **DOI:**10.1021/ic200409d
    (b) A. Biswas, L. K. Das, M. G. B. Drew, C. Diaz, A. Ghosh, *Inorg. Chem.* **2012,** *51,* 10111–10121. **DOI:**10.1021/ic300319s
    (c) S. Mandal, J. Mukherjee, F. Lloret, R. Mukherjee, Inorg. Chem. **2012**, *51*, 13148–13161. **DOI:**10.1021/ic3013848
13. M. Mitra, A. K. Maji, B. K. Ghosh, G. Kaur, A. R. Choudhury,

C.-H. Lin, J. Ribas, R. Ghosh, *Polyhedron* **2013,** *61,* 15–19. **DOI:**10.1016/j.poly.2013.05.017

14. (a) M. Maiti, D. Sadhukhan, S. Thakurta, E. Zangrando, G. Pilet, A. Bauzá, A. Frontera, B. Dede, S. Mitra, *Polyhedron* **2014**, *75*, 40–49. **DOI:**10.1016/j.poly.2014.03.005
(b) A. Guha, K. S. Banu, A. Banerjee, T. Ghosh, S. Bhattacharya, E. Zangrando, D. Das, *J. Mol. Catal. A: Chem.* **2011**, *338*, 51–57. **DOI:**10.1016/j.molcata.2011.01.025
(c) P. Kar, Y. Ida, T. Kanetomo, M. G. B. Drew, T. Ishida, A. Ghosh, *Dalton Trans.* **2015**, *44*, 9795–9804. **DOI:**10.1039/C5DT00709G
(d) P. Chakraborty, I. Majumder, K. S. Banu, B. Ghosh, H. Kara, E. Zangrando, D. Das, *Dalton Trans.* **2016**, *45*, 742–752. **DOI:**10.1039/C5DT03659C
(e) S. Mukherjee, T. Weyhermüller, E. Bothe, K. Wieghardt, P. Chaudhuri, *Dalton Trans.* **2004**, *22*, 3842–3853. **DOI:**10.1039/B410842F
(f) P. Chakraborty, S. Majumder, A. Jana, S. Mohanta, *Inorg. Chim. Acta* **2014**, *410*, 65–75. **DOI:**10.1016/j.ica.2013.10.013
15. P. K. Basu, M. Mitra, A. Ghosh, L. Thander, C.-H. Lin, R. Ghosh, *J. Chem. Sci.* **2014**, *126*, 1635–1640. **DOI:**10.1007/s12039-014-0742-5
16. (a) R. Singh, A. Banerjee, K. K. Rajak, *Inorg. Chim. Acta.* **2010**, *363*, 3131–3138. **DOI:**10.1016/j.ica.2010.05.027
(b) M. Mitra, A. K. Maji, B. K. Ghosh, P. Raghavaiah, J. Ribas, R. Ghosh, *Polyhedron* **2014**, *67*, 19–26. **DOI:**10.1016/j.poly.2013.08.064
17. (a) S. Majumder, S. Mondal, P. Lemonie, S. Mohanta, *Dalton Trans.* **2013**, *42*, 4561–4569. **DOI:**10.1039/c2dt32629a
(b) L. Mandal, S. Sasmal, H. A. Sparkes, J. A. K. Howard, S. Mohanta, *Inorg. Chim. Acta.* **2014**, *412*, 38–45. **DOI:**10.1016/j.ica.2013.12.004
(c) X. Jing, C. He, Y. Yang, C. Duan, *J. Am. Chem. Soc.* **2015**, *137*, 3967–3974. **DOI:**10.1021/jacs.5b00832
18. (a) A. Guha, T. Chattopadhyay, N. D. Paul, M. Mukherjee, S. Goswami, T. K.Mondal, E. Zangrando, D. Das, *Inorg. Chem.* **2012**, *51*, 8750–8759. **DOI:**10.1021/ic300400v
(b) S. K. Mal, M. Mitra, C. S. Purohit, R. Ghosh, *Polyhedron.* **2015**, *101*, 191–195. **DOI:**10.1016/j.poly.2015.08.039
19. A. Chatterjee, H. R. Yadav, A. R. Choudhury, A. Ali, Y. Singh, R. Ghosh, *Polyhedron* 2018, *141*, 140–146. **DOI:**10.1016/j.poly.2017.11.040
20. (a) Y. Matoba, T. Kumagai, A. Yamamoto, H. Yoshitsu, M. Sugiyama, *J. Biol. Chem.* **2006**, *281*, 8981–8990. **DOI:**10.1074/jbc.M509785200
(b) H. Decker, T. Schweikardt, F. Tuczek, *Angew. Chem. Int. Ed.* **2006**, *45*, 4546–4550. **DOI:**10.1002/anie.200601255
21. C. Citek, C. T. Lyons, E. C. Wasinger, T. D. P. Stack, *Nat. Chem.* **2012**, *4*, 317–322. **DOI:**10.1038/nchem.1284
22. Y. Thio, X. Yang, J. J. Vittal, *Dalton Trans.* **2014**, *43*, 3545–3556. **DOI:**10.1039/c3dt52829d
23. N. Biswas, S. Saha, E. Zangrando, A. Frontera, C. R. Choudhury, *Acta Chem. Slov.* **2021**, *68*, 212–221. **DOI:**10.17344/acsi.2020.6379
24. A. Bhattacharjee, S. Halder, K. Ghosh, C. Rizzoli, P. Roy, *New J. Chem***.** **2017**, *41*, 5696–5706. **DOI:**10.1039/C7NJ00846E
25. S. K. Mal, M. Mitra, H. R. Yadav, C. S. Purohit, A. R. Choudhury, R. Ghosh, *Polyhedron* **2016**, *111*, 118–122. **DOI:**10.1016/j.poly.2016.03.033
26. A. Biswas, L. K. Das, M. G. B. Drew, G. Aromí, P. Gamez, A. Ghosh, *Inorg. Chem.* **2012**, *51*, 7993–8001. **DOI:**10.1021/ic202748m
27. T. Chattopadhyay, M. Mukherjee, A. Mondal, P. Maiti, A. Banerjee, K. S. Banu, S. Bhattacharya, B. Roy, D. J. Chattopadhyay, T. K. Mondal, M. Nethaji, E. Zangrando, D. Das, *Inorg. Chem.* **2010**, *49*, 3121–3129. **DOI:**10.1021/ic901546t
28. L. K. Das, A. Biswas, J. S. Kinyon, N. S. Dalal, H. Zhou, A. Ghosh, *Inorg. Chem.* **2013**, *52*, 11744–11757. **DOI:**10.1021/ic401020m
29. T. Ghosh, J. Adhikary, P. Chakraborty, P. K. Sukul, M. S. Jana, T. K. Mondal, E. Zangrando, D. Das, *DaltonTrans.* **2014**, *43*, 841–852. **DOI:**10.1039/C3DT51419F
30. J. Adhikary, P. Chakraborty, S. Das, T. Chattopadhyay, A. Bauzá, S. K. Chattopadhyay, B. Ghosh, F. A. Mautner, A. Frontera, D. Das, *Inorg. Chem.* **2013**, *52*, 13442–13452. **DOI:**10.1021/ic401819t
31. A. Guha, K. S. Banu, S. Das, T. Chattopadhyay, R. Sanyal, E. Zangrando, D. Das, *Polyhedron.* **2013**, *52*, 669–678. **DOI:**10.1016/j.poly.2012.07.088
32. G. Borah, J. Baruah, D. Kardong, *Ind. J. Chem.* **2014**, *53A*, 1520–1525
33. W. Kabsch, *Acta Cryst. D* **2010**, *66*, 125–132. **DOI:**10.1107/S0907444909047337
34. M. C. Burla, R. Caliandro, B. Carrozzini, G. L. Cascarano, C. Cuocci, C. Giacovazzo, M. Mallamo, A. Mazzone, G. Polidori, *J. Appl. Cryst.* **2015**, *48*, 306–309. **DOI:**10.1107/S1600576715001132
35. G. M. Sheldrick, *Acta Cryst.* **2008**, *64*, 112–122. **DOI:**10.1107/S0108767307043930
36. K. Brandenburg, DIAMOND, Crystal Impact GbR, Bonn, Germany, **1999.**
37. Gaussian 09, Revision D.01; Gaussian, Inc.: Wallingford, CT, 2009. Gaussian 09, Revision D.01; Gaussian, Inc.: Wallingford, CT, **2009**.
38. GaussView, Version 5; Gaussian, Inc.: Wallingford, CT, 2009. GaussView, Version 5; Gaussian, Inc.: Wallingford, CT, **2009**
39. K. Nakamoto, Infrared and Raman Spectra of Inorganic and Coordination Compounds, Wiley, New York, 1997, vol. 23.
40. N. Beyazit, B. Catikkas, S. Bayraktar, C. Demetgül, *J. Mol. Struct.* **2016**, *1119*, 124–132. **DOI:**10.1016/j.molstruc.2016.04.047
41. R. M. El-Shazly, G. A. A. Al-Hazmi, S. E Ghazy, M. S. El-Shahawi, A. A El Asmy, *Spectrochim. Acta Part A* **2005,** *61*, 243–252. **DOI:**10.1016/j.saa.2004.02.035
42. A. Hazari, L. K. Das, R. M. Kadam, A. Bauzá, A. Frontera, A. Ghosh, *Dalton Trans.* **2015**, *44*, 3862–3876. **DOI:**10.1039/C4DT03446E
43. S. Mondal, B. Pakhira, A. J. Blake, M. G. B. Drew, S. K. Chattopadhyay, *Polyhedron* **2016**, *117*, 327–337. **DOI:**10.1016/j.poly.2016.05.052
44. (a) M. Hakimi, R. Takjoo, V. Erfaniyan, E. Schuh, F. Mohr,

Trans. Met. Chem. 2010, 35, 959–965. DOI:10.1007/s11243-010-9417-3
(b) K. Begum, E. Zangrando, M. S. Begum, C. Sheikh, R. Miyatake, *IUCrData*, **2018**, *3*, x181684. **DOI:**10.1107/S241431461801684X
(c) S. S. Khan, M. B. H. Howlader, M. C. Sheikh, R. Miyatake, E. Zangrando, *Acta Cryst.*, **2023**, *E79*, 714–717. **DOI:**10.1107/S2056989023005935

45. M. Ghosh, N. Sepay, C. Rizzoli, C. K. Ghosh, A. Banerjee, S. Saha, *New J. Chem*. **2021**, *45*, 2995–3006. **DOI:**10.1039/D0NJ04610H
46. N. Sepay, R. Mondal, M. K. Al-Muhanna, D. Saha, *New J. Chem*. **2022**, *46*, 9735–9744. **DOI:**10.1039/D2NJ00389A
47. N. Sepay, P. C. Saha, Z. Shahzadi, A. Chakraborty, U. C. Halder, *Phys. Chem. Chem. Phys*. **2021**, *23*, 7261–7270. **DOI:**10.1039/D0CP05714B
48. B. K. Biswas, S. Saha, N. Biswas, M. Chowdhury, A. Frontera, C. Rizzoli, R. R. Choudhury, C. R. Choudhury, *J. Mol. Struct*, **2020**, *1217*, 128398. **DOI:**10.1016/j.molstruc.2020.128398
49. S. Saha, N. Biswas, A. Sasmal, C. J. Gómez-Garcia, E. Garribba, A. Bauzá, A. Frontera, G. Pilet, G. M. Rosair, S. Mitra, C. R. Choudhury, *Dalton Trans*. **2018**, *47*, 16102–16118. **DOI:**10.1039/C8DT02417K
50. S. Mistri, H. Puschmann, S. C. Manna, *Polyhedron*. **2016**, *115*, 155–163. **DOI:**10.1016/j.poly.2016.05.003
51. P. Adak, B. Ghosh, A. Bauzá, A. Frontera, A. J. Blake, M. Corbella, C. D. Mukhopadhyay, S. K. Chattopadhyay, *RSC Adv*. **2016**, *6*, 86851–86861. **DOI:**10.1039/C6RA14059A
52. (a) P. Vijayan, P. Viswanathamurthi, K. Velmurugan, R. Nandhakumar, M. D. Balakumaran, P. T. Kalaichelvan, J. G. Malecki, *RSC Adv*. **2015**, *5*, 103321–103342. **DOI:**10.1039/C5RA18568H
(b) J. P. Chyn, F. L. Urbach, *Inorg. Chim. Acta* **1991**, *189*, 157–163. **DOI:**10.1016/S0020-1693(00)80184-X

Povzetek

Sintetizirali smo nov enojedrni nikljev(II) kompleks s tiosemikarbazonom (**1**), pri čemer smo kot ligand uporabili Schiffovo bazo pripravljeno iz *p*-anisaldehida in tiosemikarbazida. Spojino **1** smo karakterizirali z uporabo različnih spektroskopskih tehnik in z monokristalno rentgensko strukturno analizo. Za simulacijo elektronskih spektrov spojine **1** smo uporabili časovno odvisno teorijo gostotnih funkcionalov (TD-DFT) z uporabo modela PCM. Kompleks **1** deluje kot funkcionalni model za oksidacijo katehola, pri čemer smo katalitske lastnosti določali iz Lineweaver-Burkovega diagrama z uporabo Michaelis-Mentenovega pristopa encimske katalize z vrednostjo k_{cat} = 708 h^{-1}.